

8-2015

## Optimization of Chest Wall Hyperthermia Treatment Using a Virtual Human Chest Model


Dario B. Rodrigues  
*Thomas Jefferson University*

Mark D. Hurwitz  
*Thomas Jefferson University and Hospitals*

Paolo F. Maccarini  
*Duke University*

Paul R. Stauffer  
*Thomas Jefferson University*

Follow this and additional works at: <https://jdc.jefferson.edu/radoncfp>

 Part of the [Oncology Commons](#), and the [Radiology Commons](#)

[Let us know how access to this document benefits you](#)

---

### Recommended Citation

European Conference on Antennas and Propagation

This Article is brought to you for free and open access by the Jefferson Digital Commons. The Jefferson Digital Commons is a service of Thomas Jefferson University's [Center for Teaching and Learning \(CTL\)](#). The Commons is a showcase for Jefferson books and journals, peer-reviewed scholarly publications, unique historical collections from the University archives, and teaching tools. The Jefferson Digital Commons allows researchers and interested readers anywhere in the world to learn about and keep up to date with Jefferson scholarship. This article has been accepted for inclusion in Department of Radiation Oncology Faculty Papers by an authorized administrator of the Jefferson Digital Commons. For more information, please contact: [JeffersonDigitalCommons@jefferson.edu](mailto:JeffersonDigitalCommons@jefferson.edu).

# Optimization of Chest Wall Hyperthermia Treatment Using a Virtual Human Chest Model

Dario B. Rodrigues<sup>1</sup>, Mark D. Hurwitz<sup>1</sup>, Paolo F. Maccarini<sup>2</sup>, Paul R. Stauffer<sup>1</sup>

<sup>1</sup> Radiation Oncology Department, Thomas Jefferson University, Philadelphia PA, USA, dario.rodrigues@jefferson.edu, mark.hurwitz@jefferson.edu, paul.stauffer@jefferson.edu

<sup>2</sup> Biomedical Engineering Department, Duke University, Durham NC, USA, paolo.maccarini@duke.edu

**Abstract**—This work explores different coupling configurations (direct contact, air and water coupling) between a single 915 MHz waveguide applicator and human tissue in the setting of chest wall recurrence (CWR) of breast cancer. The objective is to treat chest wall tumours with microwave hyperthermia, while avoiding hot spots in critical areas such as scars and ribs. The best coupling configuration was a customized 24×29 cm water bolus developed by our team. It helps the applicator deliver an effective field size of 268 cm<sup>2</sup> at 1 cm depth and a penetration depth of 2-3 cm. Water bolus thickness can be adjusted during treatment (0.5-4 cm) to shift hot spot locations and thus homogenize thermal dose delivered over a 60 min hyperthermia treatment. The virtual human chest model is easily customized so it can be used as a tool for treatment planning and quality assurance testing of microwave applicator configurations.

**Index Terms**—microwave antenna, chest wall recurrence, treatment planning, breast cancer, hyperthermia.

## I. INTRODUCTION

The efficacy of adding superficial hyperthermia to radiotherapy for chest wall recurrence (CWR) of breast cancer has previously been established in randomized trials [1, 2]. However, a definite consensus towards appropriate treatment delivery has not been achieved and existing clinical guidelines are currently being redefined [3, 4]. This paper reviews the critical elements in superficial hyperthermia treatments for CWR, and presents a virtual human chest model to be used as a tool for treatment planning and quality assurance testing of different microwave applicator configurations.

The treatment planning of superficial microwave hyperthermia treatments considers three main components: applicator, coupling between applicator and tissue, and patient disease. Typical microwave applicators for these treatments operate either at 434 MHz (Europe) or 915 MHz (USA). Single and array applicators have been explored [5-7], but for clinical practice in the USA, only single waveguide applicators have been approved. The most common coupling mechanism is a water bolus. It consists of a flexible plastic bag filled with circulating deionized water at a controlled temperature. It plays a critical role since it homogenizes the radiation field and cools the skin, diffusing superficial hot spots and allowing minor adjustment of penetration depth. This becomes especially useful for low perfusion tissues such as scars that are typical in CWR and have reduced ability to dissipate heat. Several parameters of the coupling bolus must be considered: dielectric

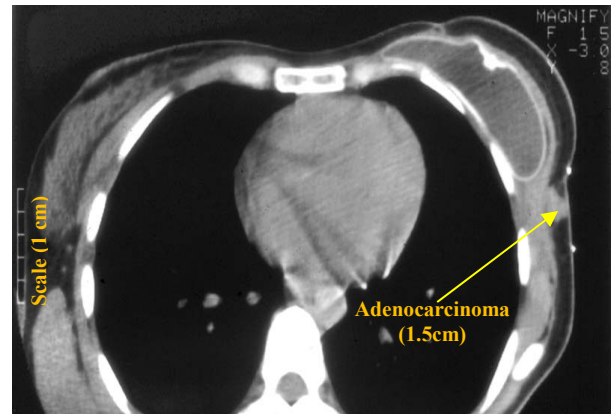


Fig. 1. Transverse CT image of a female patient with CWR of breast cancer.

properties, temperature, flow rate, shape, size, and thickness [3, 8, 9]. Finally, one must also account for human anatomy, tissue thermophysical properties [10-14] including dynamic temperature dependent blood perfusion [15, 16], and most importantly patient tolerance.

In this work, three computational models are assessed to evaluate different aspects of a superficial hyperthermia treatment. The first replicates a muscle-like homogenous phantom used to validate the computational model (model 1). The second is similar to the first but with actual human muscle properties (model 2). Finally, a “virtual human” test model is developed for treatment planning, which includes typical scars and tumours of CWR with different properties (model 3). In this model, the target temperature for hyperthermia cancer treatment is defined in the range 40-45°C [7].

## II. METHODS

### A. Experimental setup

The applicator analysed in this study is a rectangular slab-loaded waveguide with dimensions 17.4×23.6×19.6 cm (MA120, BSD Medical Corporation, Salt Lake City, Utah). The radiated fields produced by the antenna were measured with a miniature three-axis electric field probe with 1 mm step size (Model 8021 B SAR Probe, Narda Corp, Hauppauge, NY) in a tank containing a liquid muscle-like phantom. The probe provides linearized output voltage directly proportional to the total electric field squared  $|E|^2$  which is proportional to the

TABLE I. THERMAL, BIOLOGICAL AND DIELECTRIC PROPERTIES OF HUMAN TISSUES AND PHANTOM MATERIALS.

| Property<br>Tissue     | $\rho$<br>(kg/m <sup>3</sup> ) | $C_p$<br>(J/kg/K) | $k$<br>(W/m/K) | $\omega_b$<br>(kg/s/m <sup>3</sup> ) | $Q_m$<br>(W/m <sup>3</sup> ) | $s$<br>(°C <sup>2</sup> ) | $\omega_l$ | $T_{cr}$<br>(°C) | $\epsilon_r$    | $\sigma$<br>(S/m) |
|------------------------|--------------------------------|-------------------|----------------|--------------------------------------|------------------------------|---------------------------|------------|------------------|-----------------|-------------------|
| Skin (skin wet)        | 1109 [10]                      | 3391 [10]         | 0.37 [10]      | $0.97 \times F(T)$ [10]              | 1827 [10]                    | 9.2 [15]                  | 10 [15]    | 44 [15]          | 46.0 [13]       | 0.85 [13]         |
| Subcutaneous fat       | 911 [10]                       | 2348 [10]         | 0.21 [10]      | $0.52 \times F(T)$ [10]              | 461 [10]                     | 1.0 [15]                  | 12 [15]    | 45 [15]          | 5.5 [13]        | 0.05 [13]         |
| Muscle                 | 1090 [10]                      | 3421 [10]         | 0.49 [10]      | $0.75 \times F(T)$ [10]              | 1052 [10]                    | 7.9 [15]                  | 12 [15]    | 45 [15]          | 55.0 [13]       | 0.95 [13]         |
| Lung                   | 722 [10]                       | 3886 [10]         | 0.39 [10]      | $5.06 \times F(T)$ [10]              | 4483 [10]                    | 7.9 [15]                  | 12 [15]    | 45 [15]          | 36.7 [13]       | 0.66 [13]         |
| Rib                    | 1543 [10]                      | 1793 [10]         | 0.32 [10]      | $0.48 \times F(T)$ [10]              | 421 [10]                     | 1.0 [15]                  | 12 [15]    | 45 [15]          | 16.6 [13]       | 0.24 [13]         |
| Scar (skin dry)        | 1109 [10]                      | 3391 [10]         | 0.37 [10]      | -                                    | -                            | -                         | -          | -                | 41.3 [13]       | 0.87 [13]         |
| Blood                  | 1050 [10]                      | 3617 [10]         | 0.52 [10]      | -                                    | -                            | -                         | -          | -                | 61.3 [13]       | 1.54 [13]         |
| Low $\omega_b$ tumour  | 1090 [10]                      | 3421 [10]         | 0.49 [10]      | $0.58 \times F(T)$ [12]              | 1225 [12]                    | 2.0 [16]                  | 12 [16]    | 43 [16]          | 51.3 [14]       | 0.89 [14]         |
| High $\omega_b$ tumour | 1090 [10]                      | 3421 [10]         | 0.49 [10]      | $1.91 \times F(T)$ [12]              | 2267 [12]                    | 2.0 [16]                  | 12 [16]    | 43 [16]          | 56.3 [14]       | 0.97 [14]         |
| Adenocarcinoma         | 1090 [10]                      | 3421 [10]         | 0.49 [10]      | $7.63 \times F(T)$ [11]              | 3754 [12]                    | 2.0 [16]                  | 12 [16]    | 43 [16]          | 60.0 [14]       | 1.07 [14]         |
| Muscle phantom         | 1097                           | 3083              | 0.31           | -                                    | -                            | -                         | -          | -                | 46 <sup>a</sup> | 1.26 <sup>a</sup> |
| De-ionized water       | 992                            | 4176              | 0.63           | -                                    | -                            | -                         | -          | -                | 79 <sup>a</sup> | 0.18 <sup>a</sup> |

<sup>a</sup>measured.

specific absorption rate  $SAR = \sigma E^2 / 2\rho$ , where  $\sigma$  is the electrical conductivity and  $\rho$  the density of the phantom, respectively. This fluid phantom is a standard mixture of ethylene glycol and saline which matches the dielectric properties of muscle at 915 MHz: 70% laboratory grade ethylene glycol, 28% distilled water and 2% non-iodized table salt (properties on Table I).

### B. Computational model

All models include the complete structure of the slab-loaded waveguide applicator, using  $\sigma = 4.75$  for the packed crystalline sodium chloride chambers against the sidewalls. The load dimensions of models 1 (phantom) and 2 (muscle) are  $35 \times 44 \times 13$  cm and the thermophysical properties are presented in Table I. Model 3 consists of a mixture of tumour, skin, blood, necrotic tissue as well as adipose and fibroconnective tissues typical of CWR (Fig. 1). The thermophysical and biological properties of this heterogeneous tissue vary by several orders of magnitude [11, 14, 17]. Fig. 2 shows the multi-layer model 3, which includes 1.5 mm skin, 8 mm fat, 1 cm muscle, 9 cm lung and 3 ribs (bone) located 1 mm above the lung in the muscle region. This model also includes two scars ( $0.35 \times 10 \times 1$  cm) running perpendicular and parallel to the electric field (E-field) and three distinct tumours. Many different tumour geometries can be considered in CWR, including carcinomas, melanomas, and even some lymphomas. Many are diffuse disease involving skin while others are discrete nodules. Therefore, we account for one adenocarcinoma as seen in Fig. 1 (cylinder with 1.5 cm radius and height) and two elliptically shaped chest wall tumours ( $3 \times 5 \times 1.5$  cm) – Tumour L and Tumour H with low and high blood perfusion, respectively. The thermophysical properties for all tissue regions are given in Table I.

The E-field and temperature are calculated in COMSOL Multiphysics (COMSOL, Palo Alto, CA) – a finite element software – to solve the combined bioheat transfer equation and Maxwell equations [17]. The bioheat equation consists of an

extended version of the classic heat equation with a heat sink due to blood perfusion ( $\omega_b$ ), an internal heat source due to metabolism ( $Q_m$ ) and an external heat source due to absorption of microwave energy derived from the applicator ( $\rho SAR$ ). The electro-thermal model is meshed with manual settings, where the maximum mesh element size of each object is  $\lambda_{air} / \sqrt{\epsilon}$  with  $\lambda_{air}$  the wavelength in air and  $\epsilon$  the dielectric constant of the meshed object. The resulting model consists of approximately  $1 \times 10^6$  tetrahedral elements. All simulations are performed for an operating frequency of 915 MHz. The cooling bolus is embodied in a Robin boundary condition with variable  $T_{bolus}$  and fixed  $h_{bolus} = 85$  W/m<sup>2</sup>/K [3]. In the top and lateral surfaces, we impose a similar boundary condition due to air cooling with  $T_{air} = 25^\circ\text{C}$  and  $h_{air} = 5$  W/m<sup>2</sup>/K. At the bottom surface we impose a core temperature of  $T_{core} = 37^\circ\text{C}$ .

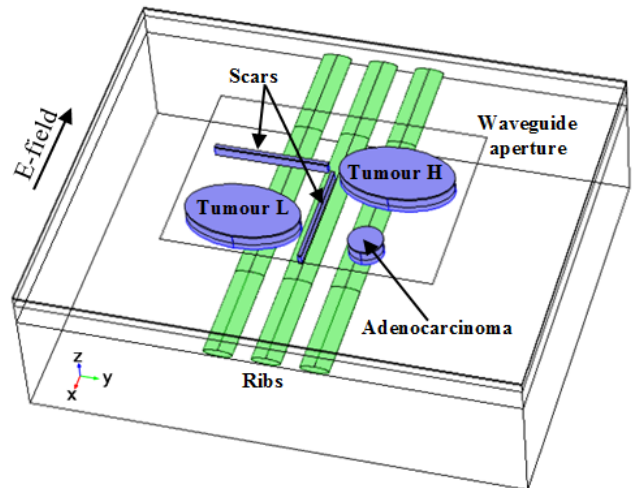


Fig. 2. Model 3 – virtual human chest model with 1.5 mm skin, 8 mm fat, 2 cm muscle, and 10 cm lung thicknesses. Lateral dimensions are  $36 \times 44$  cm. Waveguide aperture dimensions are  $17.4 \times 23.6$  cm. Tumour L and Tumour H correspond to low and high blood perfusion tumours, respectively.

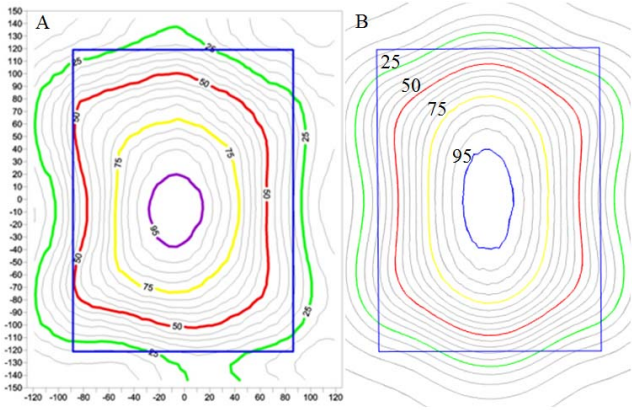


Fig. 3. Experimental (A) and simulated (B) SAR pattern at 5 mm depth in model 1 for 3 cm air coupling between applicator and liquid muscle phantom.

Finally, we account for thermoregulation. Blood perfusion, in particular, plays a critical role in hyperthermia treatments since it is a dynamic heat sink that varies with temperature [15, 16]. To account for this thermoregulatory effect, we included a temperature-dependent scaling function given by:

$$F(T) = \begin{cases} 1 + \omega_l \exp\left(-\frac{(T - T_{cr})^2}{s}\right), & T \leq T_{cr} \\ 1 + \omega_l, & T > T_{cr} \end{cases} \quad (1)$$

where  $\omega_l$  and  $s$  are curve fitting parameters derived from experimental data; and  $T_{cr}$  is a critical temperature that is tissue-specific (Table I).

### C. Parametric studies

SAR patterns of the MA120 applicator were measured and simulated at a depth of 5 mm in model 1 for four different coupling configurations: direct contact; 3 cm air coupling and no water bolus; BSD water bolus (19.4×27.6×3 cm), which integrated in a teflon frame; and a custom water bolus bag (24×29×3 cm). Water flow was approximately 3.6 l/min as controlled with the BSD 500 water conditioning system (BSD Medical Corporation, Salt Lake City, Utah). For characterization purposes, we chose to determine the effective field size (EFS) that is the area of the 50% SAR contours measured at 1 cm depth, and the penetration depth (PD) that is the distance below 1 cm at which SAR falls to 50% of that at 1 cm [5]. In model 2, the EFS and PD were determined for several different thickness of water and air coupling: 5, 13, 20, 30 and 40 mm.

## III. RESULTS

### A. Experimental validation of computational model

The experimental SAR results were measured and normalized in a plane 5 mm deep in the phantom. Simulations of all configurations in the matching model 1 are in good agreement with the measured SAR patterns. The 3 cm air gap configuration is shown in Fig. 3 as an example.

In Fig. 4, simulations of both direct contact and air coupling configurations show a Gaussian-like pattern, with 50% SAR areas of 18×18 cm<sup>2</sup> and 13×22 cm<sup>2</sup>, respectively.

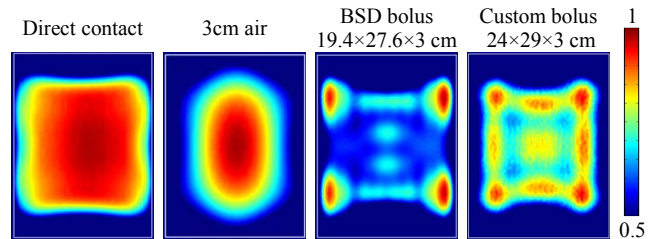


Fig. 4. Normalized SAR pattern at 5 mm depth in model 1 for four applicator configurations. The external white frame corresponds to the waveguide boundaries: 17.4×23.6 cm.

The use of a water bolus improves coupling between applicator and tissue. Both water boluses present a similar field size at 5 mm depth of approximately 16×16 cm<sup>2</sup>. However, the use of a larger water bolus bag produces a more homogenous SAR pattern that is desirable for superficial hyperthermia treatment.

### B. Characterization of different applicator configurations

The penetration depth and effective field size at 1 cm depth in model 2 are presented in Table II. The average PD is 2 cm and it is higher for water coupling due to improved impedance matching. Increasing the separation between applicator and muscle load decreases EFS for both air and water coupling. However, for water boluses thicker than 1 cm there is a non-linear behaviour, explained by SAR perturbations arising due to resonance inside the bolus [8]. Although the EFS of air coupling is higher, its centrally peaked SAR pattern is less desirable for treatment of large area CWR (Fig. 4).

### C. Heating of virtual human chest wall test phantom

In Fig. 5, we present the range of volume (dark green) and surface (light green) temperatures as well as SAR distribution (blue) for each tissue region. The following setup is typical in our clinic: bolus temperature = 42°C; bolus thickness = 13 mm (Fig. 5A) or 30 mm (Fig. 5B); input power = 160 W. The advantage of presenting both temperature and SAR together is that it emphasizes the impact on temperature increase of the quite different power deposition and thermal properties of the various tissue regions. For instance, the two tumours that differ only in blood perfusion absorb a similar SAR range, but

TABLE II. PENETRATION DEPTH AND EFFECTIVE FIELD SIZE FOR SEVERAL WATER AND AIR SEPARATIONS BETWEEN APPLICATOR AND SKIN.

| Thickness (mm)   | PD (cm) |     | EFS (cm <sup>2</sup> ) |     |
|------------------|---------|-----|------------------------|-----|
|                  | Water   | Air | Water                  | Air |
| Direct contact   | 2.3     |     | 311                    |     |
| 5                | 2.1     | 2.0 | 293                    | 401 |
| 9                | 2.0     | 1.8 | 283                    | 371 |
| 13               | 2.0     | 1.9 | 281                    | 344 |
| 20               | 2.1     | 1.9 | 266                    | 305 |
| 30               | 1.9     | 1.9 | 245                    | 287 |
| 40               | 2.0     | 1.9 | 240                    | 278 |
| BSD bolus (30mm) | 1.6     | -   | 264                    | -   |



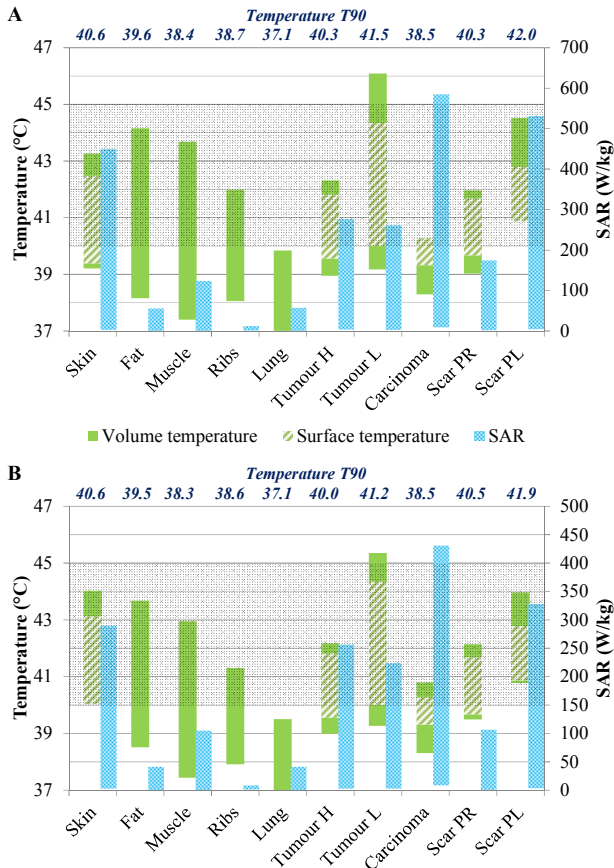


Fig. 5. Temperature and SAR distribution for all tissues in model 3 with  $T_{bolus} = 42^{\circ}\text{C}$ , bolus thickness = 13 mm (A) and 30 mm (B); antenna power = 160 W (Tumor H = tumor with high blood perfusion; Tumor L = tumor with low blood perfusion; Scar PL = parallel scar; Scar PR = perpendicular scar). Muscle, skin, fat and rib temperatures are taken from the effective heating volumes limited by the waveguide boundaries ( $17.4 \times 23.6$  cm).  $T_{90}$  is presented above the graph.

have a  $4^{\circ}\text{C}$  difference in maximum temperature. The adenocarcinoma absorbs even more energy (higher SAR) due to possible resonance effects within its 1.5 cm structure. However, this did not produce tumour temperatures in the desired  $40\text{--}45^{\circ}\text{C}$  range (shaded) due to the very high perfusion ( $7.63 \text{ kg/s/m}^3$ ) which represents a worst case of tissue properties [11]. Nonetheless, the two large tumours (L and H) were the primary targets for the treatment since they are centered in the applicator. These tumours achieve a  $T_{90}$  of  $41.5^{\circ}\text{C}$  (tumour L) and  $40.3^{\circ}\text{C}$  (tumour H) for 13 mm bolus thickness, meaning that 90% of the tumour exceeds the  $T_{90}$  temperature [17]. The remaining 10% of tumor absorbs less energy as the SAR pattern falls off rapidly at the tumor edges.

In Fig. 5, separate reporting of surface temperature range (light green) enhances understanding of deeper temperatures in the same tissue regions. In the clinic, eight measurements are typically collected per treatment. Due to the cooling effect of the bolus and higher power deposition at the surface, the temperature differentials are significant. They range from  $1^{\circ}\text{C}$  (adenocarcinoma) to  $4.3^{\circ}\text{C}$  (tumour H) in terms of surface temperature, but can reach  $7^{\circ}\text{C}$  (tumour L) in terms of volume temperature differential.

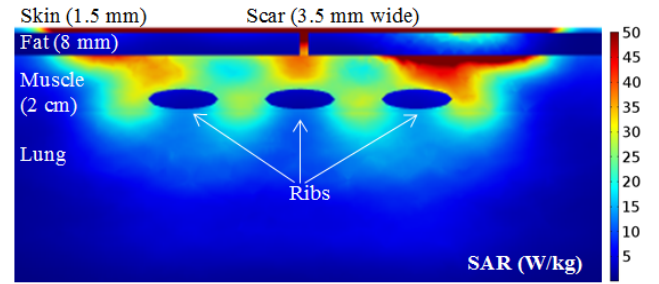


Fig. 6. Transverse plane of SAR pattern across human chest wall model 3.

The effect of constructive interference due to reflections at the sharply contrasting rib/muscle dielectric interfaces can be observed in Fig. 6. In this model, SAR from the 915 MHz field does not cause overheating of surface tissues since the ribs are 2.5 cm deep. For mastectomy patients that often have less than 1-1.5 cm tissue overlying the ribs, hot spots may result above and between the ribs.

#### IV. DISCUSSION

In this work, we validate a new treatment planning model for the BSD MA120 waveguide applicator and characterize four applicator/bolus setups for superficial CWR treatments. Current tools allow segmentation of patient-specific anatomical models [18], but these are time consuming and not yet practical for routine planning. We use a virtual human chest wall model as a tool for quick assessment of different treatment configurations. The model includes all structures typical of chest wall recurrence, and is easily customized.

Although this study addresses a single applicator, it illuminates several mechanisms available to adjust temperature distribution under a microwave applicator. The air coupling was implemented since it is relevant in some extreme cases, where patients present open wounds with active bleeding and are intolerant to pressure. However, the use of water bolus is always preferable in order to control skin temperature.

In Fig. 5, temperature and SAR distributions are presented for different bolus thicknesses. By increasing the thickness from 13 mm to 30 mm, the maximum temperatures of healthy tissues decrease up to  $0.7^{\circ}\text{C}$  while maintaining tumours  $T_{90}$  within the range  $40\text{--}45^{\circ}\text{C}$ . In practice, when placed on a contoured chest, the bolus thickness can reach 4-5 cm at its borders, while in the centre it may be less than 1 cm thick. Clearly, variations in bolus thickness contribute to hot spots, but those hot spots can be shifted around under the aperture as shown in Fig. 4 to homogenize thermal dose delivered over a 60 min treatment.

The development of hot spots is unavoidable in HT treatment, and in extreme cases might lead to pain and blisters. Overheating may occur at bone/muscle and fat/muscle interfaces, and in poorly perfused tissues such as scars, grafts and the interior of necrotic tumours. The scars of model 3, which run parallel and perpendicular to the electric field, demonstrate that power absorption and tissue temperature are very different, even though both scars are located within the

50% SAR contour. In fact, parallel orientation produces preferential heating of scar tissue, suggesting rotation of the applicator to avoid preferential accumulation of heat in the scars.

In this work we accounted for tissue-specific temperature dependent perfusion. Without this effect, only 60 W were required to heat the model 3 tumour target regions into the desired 40-45°C range. However, after accounting for thermoregulation, the heat dissipation increased and more power was required. The power used to obtain the distributions in Figs. 5 and 6 was 160 W, which agrees with the 120-180 W range used clinically for the MA120.

Finally, penetration depth is a parameter that has different definitions in the literature. If we apply the definition traditionally used in hyperthermia [5], the penetration depth is about 2 cm for different applicator configurations (Table II). However, others have defined PD as the depth at which the SAR becomes  $1/e^2$  of its value at the surface. In this case the effective PD is 3 cm, which is consistent with 3 cm deep tissues (lung) reaching 40°C (Fig. 5). Ultimately, the temperature and consequently thermal dose distribution is what is most relevant clinically [7, 17]. The relevance of temperature is sometimes embodied in  $T_{90}$ , which is useful to quantify the temperature distribution. However, thermal modeling assessment of complete temperature ranges for all tissues is a valuable tool to predict the location of hot spots and thus improve treatment quality.

In summary, the virtual human chest wall model facilitates instructive treatment planning that can be easily adjusted to model individual anatomies, such as different thicknesses and depths of fat, scars, tumours and ribs. In our clinic, the majority of patients present disease dispersed within the top 1-2 cm. Deeper tumours can also be heated by increasing input power and decreasing the bolus temperature [3].

## V. CONCLUSIONS

A simplified 3D computer model was developed for the study of superficial hyperthermia treatments with a single microwave waveguide applicator. All clinically relevant structures were included in the model. Although single waveguide applicators are fairly simple, there are several parameters that can be adjusted to minimize hot spots that cause pain and blisters. While heating pattern peaks are unavoidable, they can be shifted during treatment by varying bolus temperature and thickness. The custom water bolus bag demonstrated better performance than the teflon frame bolus supplied with the applicator. The proposed temperature and SAR range analysis facilitates rapid global assessment of CWR treatment quality. The presented simplified computer model can then be integrated in routine treatment planning into quality assurance (QA) practice for improved therapy in the clinic.

## ACKNOWLEDGMENT

The authors acknowledge BSD Medical Corporation (Salt Lake City, Utah) for providing details on waveguide construction and initial motivation for the project.

## REFERENCES

- [1] C. C. Vernon, J. W. Hand, S. B. Field, D. Machin, J. B. Whaley, *et al.*, "Radiotherapy with or without hyperthermia in the treatment of superficial localized breast cancer: Results from five randomized controlled trials," *Int. J. Radiat. Oncol. Biol. Phys.*, vol. 35, no. 4, pp. 731-744, July 1996.
- [2] E. L. Jones, J. R. Oleson, L. R. Prosnitz, T. V. Samulski, Z. Vujaskovic, *et al.*, "Randomized trial of hyperthermia and radiation for superficial tumors," *J. Clin. Oncol.*, vol. 23, no. 13, pp. 3079-3085, May 2005.
- [3] M. L. Van der Gaag, M. de Bruijne, T. Samaras, J. Van der Zee, and G. C. Van Rhoon, "Development of a guideline for the water bolus temperature in superficial hyperthermia," *Int. J. Hyperthermia*, vol. 22, no. 8, pp. 637-656, December 2006.
- [4] M. de Bruijne, J. Van der Zee, A. Ameziane, and G. C. Van Rhoon, "Quality control of superficial hyperthermia by treatment evaluation," *Int. J. Hyperthermia*, vol. 27, no. 3, pp. 199-213, May 2011.
- [5] G. C. Van Rhoon, P. J. M. Rietveld, and J. Van der Zee, "A 433 MHz lucite cone waveguide applicator for superficial hyperthermia," *Int. J. Hyperthermia*, vol. 14, no. 1, pp. 13-27, January 1998.
- [6] J. C. Kumaradas, and M. D. Sherar, "Edge-element based finite element analysis of microwave hyperthermia treatments for superficial tumours on the chest wall," *Int. J. Hyperthermia*, vol. 19, no. 4, pp. 414-430, July 2003.
- [7] P. R. Stauffer, P. Maccarini, K. Arunachalam, O. Craciunescu, C. Diederich, *et al.*, "Conformal microwave array (CMA) applicators for hyperthermia of diffuse chest wall recurrence," *Int. J. Hyperthermia*, vol. 26, no. 7, pp. 686-698, October 2010.
- [8] K. Arunachalam, P. F. Maccarini, O. I. Craciunescu, J. L. Schlorff, and P. R. Stauffer, "Thermal characteristics of thermobrachytherapy surface applicators for treating chest wall recurrence," *Phys. Med. Biol.*, vol. 55, no. 7, pp. 1949-1969, April 2010.
- [9] M. de Bruijne, T. Samaras, J. F. Bakker, and G. C. Van Rhoon, "Effects of waterbolus size, shape and configuration on the SAR distribution pattern of the Lucite cone applicator," *Int. J. Hyperthermia*, vol. 22, no. 1, pp. 15-28, January 2006.
- [10] P. A. Hasgall, E. Neufeld, M. C. Gosselin, A. Klingenböck, and N. Kuster, "IT'IS Database for thermal and electromagnetic parameters of biological tissues," V.2.5, August 2014. [www.itis.ethz.ch/database](http://www.itis.ethz.ch/database).
- [11] R. K. Jain, and K. Wardharty, "Tumor blood-flow - characterization, modifications, and role in hyperthermia," *IEEE Trans. Sonics Ultrason.*, vol. 31, no. 5, pp. 504-526, September 1984.
- [12] P. Vaupel, F. Kallinowski, and P. Okunieff, "Blood-flow, oxygen and nutrient supply, and metabolic microenvironment of human tumors - A review," *Cancer Res.*, vol. 49, no. 23, pp. 6449-6465, December 1989.
- [13] S. Gabriel, R. W. Lau, and C. Gabriel, "The dielectric properties of biological tissues: III. Parametric models for the dielectric spectrum of tissues," *Phys. Med. Biol.*, vol. 41, no. 11, November 1996.
- [14] M. Lazebnik, D. Popovic, L. McCartney, C. B. Watkins, M. J. Lindstrom, *et al.*, "A large-scale study of the ultrawideband microwave dielectric properties of normal, benign and malignant breast tissues obtained from cancer surgeries," *Phys. Med. Biol.*, vol. 52, no. 20, pp. 6093-6115, October 2007.
- [15] T. Drizdal, P. Togni, L. Visek, and J. Vrba, "Comparison of Constant and Temperature Dependent Blood Perfusion in Temperature Prediction for Superficial Hyperthermia," *Radioengineering*, vol. 19, no. 2, pp. 281-289, June 2010.
- [16] K. S. Cheng, Y. Yuan, Z. Li, P. R. Stauffer, P. Maccarini, *et al.*, "The performance of a reduced-order adaptive controller when used in multi-antenna hyperthermia treatments with nonlinear temperature-dependent perfusion," *Phys. Med. Biol.*, vol. 54, no. 7, pp. 1979-1995, April 2009.
- [17] M. M. Paulides, P. R. Stauffer, E. Neufeld, P. F. Maccarini, A. Kyriakou, *et al.*, "Simulation techniques in hyperthermia treatment planning," *Int. J. Hyperthermia*, vol. 29, no. 4, pp. 346-357, June 2013.
- [18] M. Linthorst, T. Drizdal, H. Joosten, G. C. van Rhoon, and J. van der Zee, "Procedure for Creating a Three-Dimensional (3D) Model for Superficial Hyperthermia Treatment Planning," *Strahlenther. Onkol.*, vol. 187, no. 12, pp. 835-841, December 2011.